Global ballistic acceleration in a bouncing-ball model

Tiago Kroetz,[1] André L. P. Livorati,[2,3] Edson D. Leonel,[3,4] and Iberê L. Caldas[2]
[1]*Universidade Tecnológica Federal do Paraná, Pato Branco, Paraná, Brazil*
[2]*Instituto de Física, Universidade de São Paulo, São Paulo, São Paulo, Brazil*
[3]*Departamento de Física, Universidade Estadual Paulista, Rio Claro, São Paulo, Brazil*
[4]*Abdus Salam International Center for Theoretical Physics, Strada Costiera 11, 34151 Trieste, Italy*
(Received 7 April 2015; published 6 July 2015)

The ballistic increase for the velocity of a particle in a bouncing-ball model was investigated. The phenomenon is caused by accelerating structures in phase space known as accelerator modes. They lead to a regular and monotonic increase of the velocity. Here, both regular and ballistic Fermi acceleration coexist in the dynamics, leading the dynamics to two different growth regimes. We characterized deaccelerator modes in the dynamics, corresponding to unstable points in the antisymmetric position of the accelerator modes. In control parameter space, parameter sets for which these accelerations and deaccelerations constitute structures were obtained analytically. Since the mapping is not symplectic, we found fractal basins of influence for acceleration and deacceleration bounded by the stable and unstable manifolds, where the basins affect globally the average velocity of the system.

DOI: 10.1103/PhysRevE.92.012905 PACS number(s): 05.45.Pq, 05.45.Tp

I. INTRODUCTION

Nowadays, one of the most embracing areas of interest among physicists and mathematicians is the modeling of dynamical systems [1]. In particular, low-dimensional systems are very suitable despite the simple modeling. These systems can present a very complex dynamics leading to a rich variety of nonlinear phenomena, considering either dissipative and nondissipative dynamics [2–5].

In 1949, Fermi [6] proposed a mechanism as an attempt to explain the origin of the high energies of the cosmic rays. Fermi claimed that particles, which interacted with oscillating magnetic fields present in the cosmos, would in the average exhibit a gain of energy. This unlimited growth of energy is denominated Fermi acceleration (FA). In the literature, FA applications can be found in several areas as plasma physics [7,8], astrophysics [9–11], atom optics [12–14], and especially in billiard dynamics [15–20]. The FA phenomenon is mainly associated with normal diffusion in phase space, where there is a velocity growth proportional to $\sqrt{t}$. However, one can still find different regimes of growth, as exponential [21–24], or with a slower power law growth, where stickiness phenomenon [25] plays the role of a slowing mechanism for FA.

The model under study in this paper is the so called bouncing-ball model [26–28], where basically there is a free particle suffering elastic collisions with a vibrating platform under the influence of a constant gravitational field. In the nondissipative version and depending on the initial conditions and control parameters, the bouncing ball presents unlimited energy growth [2]. Despite the simple dynamics, applications for this model can be found in dynamic stability in human performance [29], vibration waves in a nanometric-sized mechanical contact system [30], granular materials [31,32], experimental devices concerning normal coefficient of restitution [33], mechanical vibrations [34,35], anomalous transport and diffusion [36], thermodynamics [37], chaos control [38,39], among others.

In this paper, we investigate the ballistic increase of the velocity in the bouncer model, where resonances, known as accelerator modes (AM) (or ballistic modes) [40–45], drastically influence transport and diffusion properties [46–48]. We observed that accelerating structures in phase space lead to a regular and monotonic increase of velocity, hence differing from the "regular FA" [25]. Complementary to the AM, we find unstable modes in the antisymmetric position, that we called deaccelerator modes (DM) [46]. We obtain analytically the range of the control parameter where both accelerating and deaccelerating structures are present in phase space, classifying them with multiple periods of acceleration and bifurcations. Our numerical results are in good agreement with the analytical predictions. Analyzing the dynamics considering the modulated velocity axis, we observe fractal-like basins delimited by the stable manifolds. They indeed affect globally the average velocity of the system.

The organization of the paper follows: In Sec. II, we describe the dynamics of the bouncing-ball model, in both complete and simplified approaches. Section III is devoted to the numerical and analytical analysis of the ballistic FA behavior of the AM. In Sec. IV, we investigate the chaotic properties of both AM and DM, characterizing their influence basins. Finally, in Sec. V we draw some final remarks and conclusions.

II. MODEL

This section is devoted to describe the bouncing-ball model for both complete and simplified dynamics. A schematic view of the bouncer model is shown in Fig. 1.

A particle under a constant gravitational field suffers repeated impacts with an oscillatory platform, whose position is given by $x_w(t) = A[\cos(\omega t + \varphi) - 1]$, where A is the amplitude of the platform oscillation, ω is the angular frequency, and φ is the oscillation initial phase.

The position of the particle between impacts is given by the free fall equation $x_p(t) = h_0 + vt - gt^2/2$, where h_0 is the vertical position from which the particle was previously

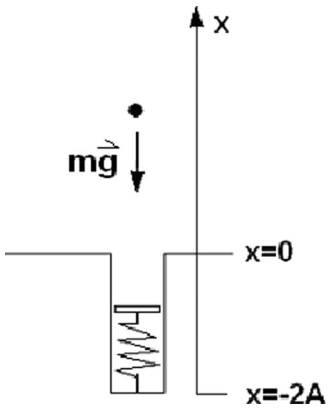

FIG. 1. Schematic view of bouncer model.

launched by the platform, v is the launch velocity, t is the time elapsed since the last impact, and g is the gravitational acceleration. The instants of impacts are obtained by equating the platform position and the particle position $x_w(t) = x_p(t)$.

A. Complete model

Considering elastic collisions, the new launch velocity will be given by the negative relative velocity between the particle and the platform just before the impact. Applying this procedure in a recurrence way, it is possible to obtain a discrete map that represents the particle velocity v_n and the phase of platform movement φ_n after the nth impact. The time interval t_{n+1} and the phase difference between two consecutive impacts are related by $t_{n+1} = (\varphi_{n+1} - \varphi_n)/\omega$. Therefore, a discrete map that describes the complete bouncer model is written as

$$\begin{aligned} &A[\cos(\varphi_n) - \cos(\varphi_{n+1})] + v_n(\varphi_{n+1} - \varphi_n)/\omega \\ &\quad -g(\varphi_{n+1} - \varphi_n)^2/2\omega^2 = 0, \\ &v_{n+1} = -v_n + g(\varphi_{n+1} - \varphi_n)/\omega - 2A\omega\sin(\varphi_{n+1}). \end{aligned} \quad (1)$$

Since the first mapping Eq. (1) is transcendental, it must be solved numerically at each collision.

The control parameters A, ω, and g are not independent. Rewriting the map in terms of a dimensionless velocity given by $V_n = \omega v_n/(\pi g)$ and a dimensionless parameter $K = \omega^2 A/(\pi g)$, which is physically interpreted as a ratio between accelerations of the moving platform and the gravitational field, we find a new map with only one control parameter K related to A, ω, and g:

$$\begin{aligned} &K[\cos(\varphi_n) - \cos(\varphi_{n+1})] + V_n(\varphi_{n+1} - \varphi_n) \\ &\quad -(\varphi_{n+1} - \varphi_n)^2/2\pi = 0, \\ &V_{n+1} = -V_n + (\varphi_{n+1} - \varphi_n)/\pi - 2K\sin(\varphi_{n+1}). \end{aligned} \quad (2)$$

The phase space volume element transforms according to the determinant of the Jacobian matrix, whose elements are given by the partial derivatives of map coordinates. The partial derivatives of φ_{n+1} are obtained by indirect differentiation of the first expression of map (2) followed by some algebra in order to isolate the terms. These expressions are written as

$$\frac{\partial\varphi_{n+1}}{\partial\varphi_n} = \frac{V_n - (\varphi_{n+1} - \varphi_n)/\pi + K\sin(\varphi_n)}{V_n - (\varphi_{n+1} - \varphi_n)/\pi + K\sin(\varphi_{n+1})}, \quad (3)$$

$$\frac{\partial\varphi_{n+1}}{\partial V_n} = \frac{-\pi(\varphi_{n+1} - \varphi_n)}{V_n - (\varphi_{n+1} - \varphi_n)/\pi + K\sin(\varphi_{n+1})}, \quad (4)$$

$$\frac{\partial V_{n+1}}{\partial\varphi_n} = \frac{\partial\varphi_{n+1}}{\partial\varphi_n}[1/\pi - 2K\cos(\varphi_{n+1})] - 1/\pi, \quad (5)$$

$$\frac{\partial V_{n+1}}{\partial V_n} = \frac{\partial\varphi_{n+1}}{\partial V_n}[1/\pi - 2K\cos(\varphi_{n+1})] - 1. \quad (6)$$

Therefore, the Jacobian determinant is given by

$$\det(J) = \frac{V_n + K\sin(\varphi_n)}{V_{n+1} + K\sin(\varphi_{n+1})}. \quad (7)$$

As can be seen in Eq. (7), the Jacobian depends on the dynamical variables. As a consequence, the system cannot be considered conservative neither dissipative since J can be greater than 1 or less than 1 for distinct regions of the phase space. This result will be further explained in Sec. IV A.

B. Simplified model

The simplified model is defined considering the platform position fixed but exchanging momentum with the particle at each impact as if it was moving. Assuming this approximation, the time elapsed between consecutive impacts can be easily found depending only of the velocity V_n. So, considering $(\varphi_{n+1} - \varphi_n) = 2\pi V_n$, the simplified bouncer model is written as

$$\begin{aligned} \varphi_{n+1} &= \varphi_n + 2\pi V_n, \\ V_{n+1} &= |V_n - 2K\sin\varphi_{n+1}|. \end{aligned} \quad (8)$$

The simplified bouncer model defined by Eqs. (8) is symplectic, as one can easily check. Although the simplified model does not correspond to the correct dynamics of a ball bouncing in a moving floor, it can be useful to evaluate analytical calculations about the position and stability of the fixed points.

III. FERMI ACCELERATION

In this section, we describe the unlimited energy growth experienced by the particle during the dynamics. As already known in the literature [2,25], for $K = 0$, the system is integrable, and when we increase K, there is a phase transition from local chaos to global chaos. Such transition is crucial for the FA phenomenon to occur. Here, we have the destruction of the invariant spanning curves, allowing the union of the local chaotic seas, so a chaotic orbit has a "free path" to diffuse along the velocity axis.

A. Numerical evidences

Due to the property of diffusion in phase space for global chaotic dynamics, we see a tendency for the velocity to grow in the average as the dynamics, as function of the number of collisions, is evolved. Such behavior is shown in Fig. 2, for several values of K in the global chaos cases, iterated until 10^7

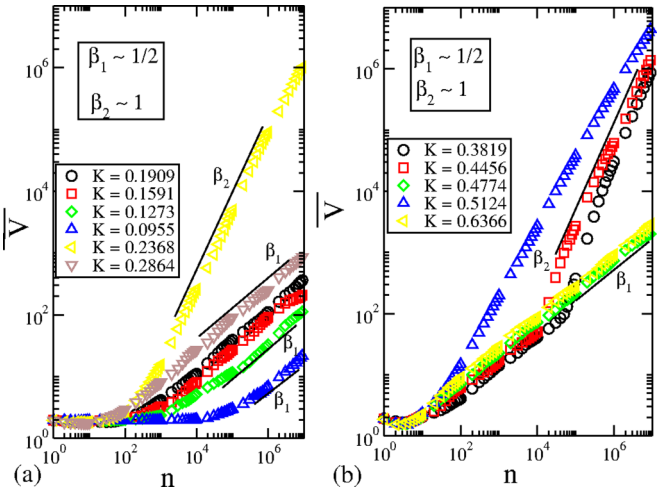

FIG. 2. (Color online) Evolution of the average velocity for different values of the parameter K. One can see two regimes of growth. Some curves grow with a power law exponent $\beta_1 \approx \frac{1}{2}$, and others grow with exponent $\beta_2 \approx 1$. In particular in (b), we may see a transition from one growth behavior to another growth regime for $K = 0.3819$ and 0.4456.

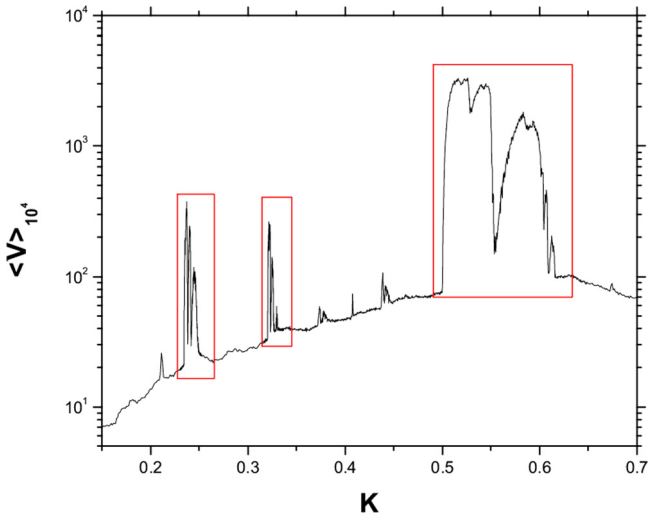

FIG. 3. (Color online) Particle average velocity evaluated in 10^4 iterations as a function of the parameter K. The peaks represent the influence of the AM in the dynamics.

collisions. For this, we define the average velocity as

$$\overline{V} = \frac{1}{M}\sum_{j=1}^{M}\overline{V_j}(n,K), \tag{9}$$

where M represents an ensemble of 5000 different initial conditions and $\overline{V_j}(n,K)$ is expressed by

$$\overline{V_j}(n,K) = \frac{1}{n}\sum_{i=1}^{n} V_i, \tag{10}$$

with n representing the iteration (collision) number.

As shown in Fig. 2, there are two distinct growing regimes. In one of them, the average velocity grows as a function of n according to a power law with exponent $\beta_1 \approx \frac{1}{2}$. The other growing regime obeys also a power law but with a different exponent $\beta_2 \approx 1$, which means a linear growth. In particular, there are some values of K that present a transition from one growth regime to another one, as shown in Fig. 2(b). Also, there are different ranges for the parameter K which exhibit a growth in the average velocity in a linear way.

In order to investigate the dependence of control parameter K on the growth of average velocity, we compute $\langle V\rangle_{10^4}$ by Eq. (9) at the end of 10^4 impacts for different values of K. We do this considering an ensemble of 5000 initial conditions at the same value of V at the low energy region and uniformly distributed in $\varphi \in [0,2\pi]$. The result can be seen in Fig. 3, and reveals that for some specific values of K the growth of average velocity is greatly favored. For the other cases of K the acceleration happens as an ordinary manner. The peaks in Fig. 3 are given by the influence of the AM in the system dynamics.

In Figs. 4(a)–4(c), we depicted the amplifications of the most pronounced peaks in the range of K investigated. It is possible to see in these figures a fine structure on the quantity $\langle V\rangle_{10^4}$. This feature indicates some metamorphosis suffered by the AM as we vary K. These will be better explained in Sec. III B, where analytical and numerical results confirm this scenario.

There is a qualitative difference on the dynamics exhibited by the system when the gain of velocity happens as a FA and as an AM. To clarify this difference, we show in Fig. 5 the dimensionless vertical positions H of the particle and of the platform as a function of time. The variable H associated with particle and platform is related with the vertical distance from the floor until the particle by means of $\omega^2 x_p(t)/\pi g$ and until the vibrating platform by means of $\omega^2 x_w(t)/\pi g$, respectively. In the case of Fig. 5(a), we select a value of K for which there is absence of AM. As can be seen for this case, the heights reached by the particle do not increase always after each impact, but in the average after several impacts, a growth can be observed. In contrast, for the AM shown in Fig. 5(b), the gain of potential energy is always ascendent. The magnifications included in each figure reveal the reason for this difference. It resides in the fact that the AM is a very special kind of dynamics where the impacts always occur for an ascendent movement of the platform [shown in red (gray)], as can be seen in magnification of Fig. 5(b). For the conventional FA, the impacts sometimes occur with the platform in a descendent movement and this promotes an instantaneous loss of energy, as can be seen in magnification of Fig. 5(a).

B. Stability estimation

In this section, we use the simplified approach to localize the position of the AM in phase space and estimate the stability of these structures as the control parameter K is varied. In the phase space, the AM consists of regular and repetitive jumps in the V direction. The simplest case happens when the mapping leads one point in phase space to another at same value of φ and shifted in the V direction by adding an integer l. We designate this kind of dynamics as period-1 AM with step size l. For the sake of simplicity we adopt $l = 1$ in this work without loss of generality. The period of the AM refers to the

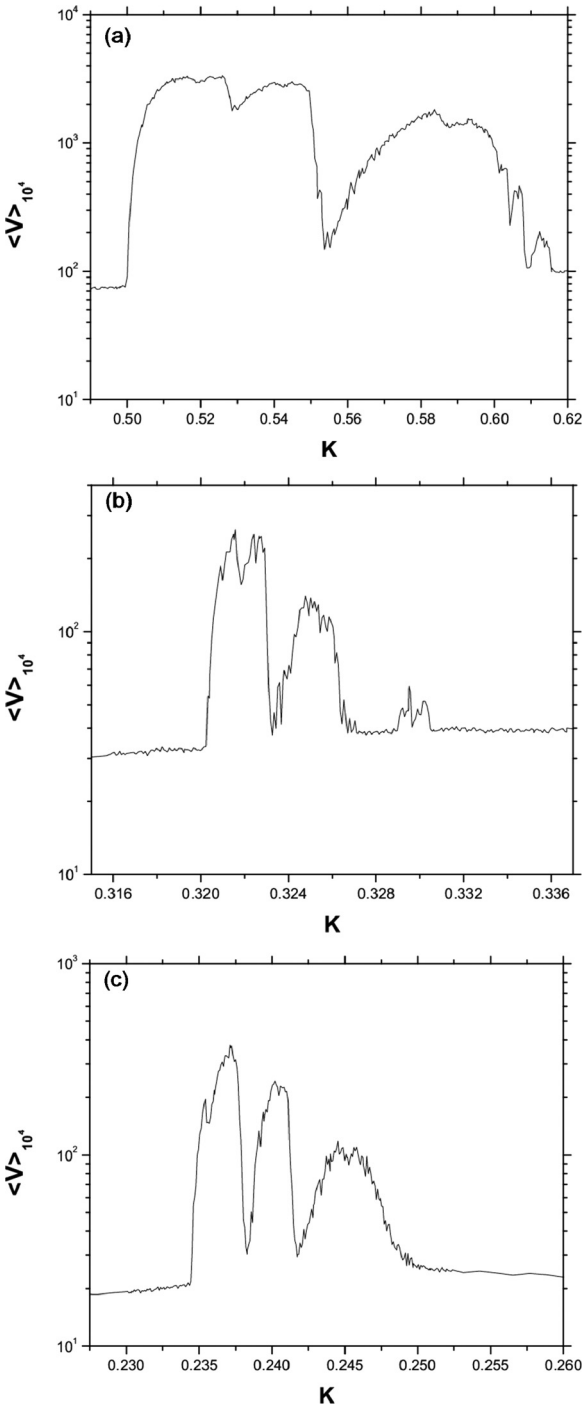

FIG. 4. Amplifications of Fig. 3 around K values corresponding to AM of (a) period-1, (b) period-2, and (c) period-4.

number of map iterations until a repetition of coordinates in a modulated phase space. Using the simplified map described by Eqs. (8) we obtain the relation for the AM coordinates $V_{n+1} - V_n = 1 = -2K \sin(\varphi_{n+1})$. If we impose an artificial periodicity along the V direction in the phase space, the period-1 AM is indistinguishable from a period-1 fixed point. The map (8) provides the position of the period-1 AM center as

$$V^{ac} = 1, \tag{11}$$

$$\varphi^{ac} = \arcsin(-1/2K). \tag{12}$$

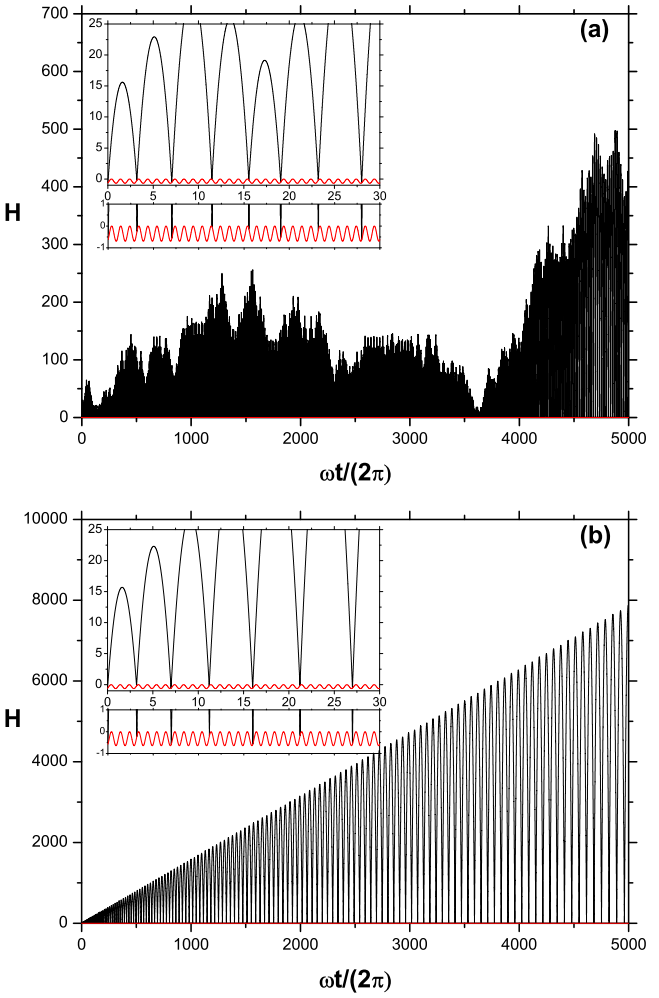

FIG. 5. (Color online) Dimensionless position (H) correspondent to the particle in black and correspondent to the vibrating platform in red (gray) as a function of dimensionless time for a dynamics for initial conditions $\varphi_0 = -2.48$, $V_0 = 3.22$ and (a) $K = 0.35$ during 700 impacts and (b) $K = 0.322$ during 130 impacts. In each figure it is possible to see a magnification of horizontal scale revealing the platform positions at each impact.

To determine the stability of the period-1 AM, we linearize the system around the position (V^{ac},φ^{ac}) via the Jacobian matrix calculated at this point. The calculation of eigenvalues leads to a characteristic expression as follows:

$$P(\lambda) = \det\begin{pmatrix} 1-\lambda & 2\pi \\ -2K\cos\varphi^{ac} & 1-4\pi K\cos\varphi^{ac}-\lambda \end{pmatrix},$$

$$P(\lambda) = \lambda^2 - \lambda(2 - 4\pi K\cos\varphi^{ac}) + 1 = 0. \tag{13}$$

The stability condition will be satisfied since the eigenvalues are complex (elliptical fixed points). So, we may obtain

$$|2 - 4\pi K\cos\varphi^{ac}| < 2 \;\rightarrow\; 0 < 4\pi K\cos\varphi^{ac} < 4. \tag{14}$$

Replacing Eq. (12) on the relation given by Eq. (14) we can express the stability condition of the period-1 AM as a function of parameter K:

$$0.5 < K < \sqrt{1/\pi^2 + 1/4}. \tag{15}$$

The range of the parameter K calculated by the simplified model corresponds to the AM shown in Fig. 4(a). Although Eq. (15) and the numerical result shown in Fig. 4(a) refer to different models, the agreement between them reveals that the simplified model is efficient to determine the position and stability of AM in complete bouncer model.

To corroborate the assumption that the complete model behavior indicated in Figs. 4(a)–4(c) corresponds to the AM obtained by means of simplified model, we perform the calculation of stability of the period-2 AM in order to compare with Fig. 4(b). To do this we need to obtain a second iterated map version of map given in Eq. (8). This procedure leads to

$$\varphi_{n+2} = \varphi_n + 4\pi V_n - 4\pi K \sin(\varphi_n + 2\pi V_n),$$
$$V_{n+2} = V_n - 2K \sin(\varphi_n + 2\pi V_n) - 2K \sin\varphi_{n+2}. \quad (16)$$

This version of the map does not allow us to find an analytical expression for the position (V^*,φ^*) of the period-2 AM since we have a transcendental equation depending on V^*. However, we can find, after some algebra, the relation $\sin(\varphi^*) = (1-2V^*)/2K$ between the period-2 AM coordinates. The Jacobian of the map in Eq. (16) is written in terms of the following partial derivatives:

$$\frac{\partial\varphi_{n+2}}{\partial\varphi_n} = 1 - 2B, \quad (17)$$
$$\frac{\partial\varphi_{n+2}}{\partial V_n} = 4\pi - 2\pi B, \quad (18)$$
$$\frac{\partial V_{n+2}}{\partial\varphi_n} = -B/\pi - A(1-2B)/\pi, \quad (19)$$
$$\frac{\partial V_{n+2}}{\partial V_n} = 1 - 2B - 4A(1-B), \quad (20)$$

where the auxiliary variables are $A = 2\pi K\cos(\varphi^*)$, $B = 2\pi K\cos(\varphi^* + 2\pi V^*)$. The eigenvalues of the Jacobian matrix at the position of the period-2 AM are given by

$$\lambda = 1 + 2(AB - A - B) \pm 2\sqrt{f(\varphi^*,V^*)}, \quad (21)$$

where $f(\varphi^*,V^*)$ is an expression that must be negative for the eigenvalue to become complex. So, we obtain

$$f(\varphi^*,V^*) = A^2B^2 + A^2 + B^2 + 3AB - 2(AB^2 + A^2B) - A - B. \quad (22)$$

As we cannot analytically find the position (V^*,φ^*) dependent on K, we adopt as procedure to follow numerically these coordinates as the control parameter K is varied. After replacing the values of (V^*,φ^*) numerically obtained in the expression of Eq. (22), we plot the dependence of $f(\varphi^*,V^*)$ with the parameter K in Fig. 6.

The range of K, where $f(\varphi^*,V^*)$ is negative, corresponds to a period-2 AM. This range is verified in Fig. 4(b) as a large increase on the $\langle V\rangle_{10^4}$ dependence. Again, we conclude that the behavior of complete model shown in Figs. 4(a)–4(c) is due to AM, and the stability of these modes can be estimated by the simplified model. However, we can observe some fluctuations and drastic decreases of the quantity $\langle V\rangle_{10^4}$ along the AM range of stability. Also, the curves in Figs. 4(a) and 4(b) extend further than predicted by Eqs. (15) and (22), respectively. The explanation to these features is done by the analysis of the bifurcations and the resonances around islands of acceleration in the simplified model.

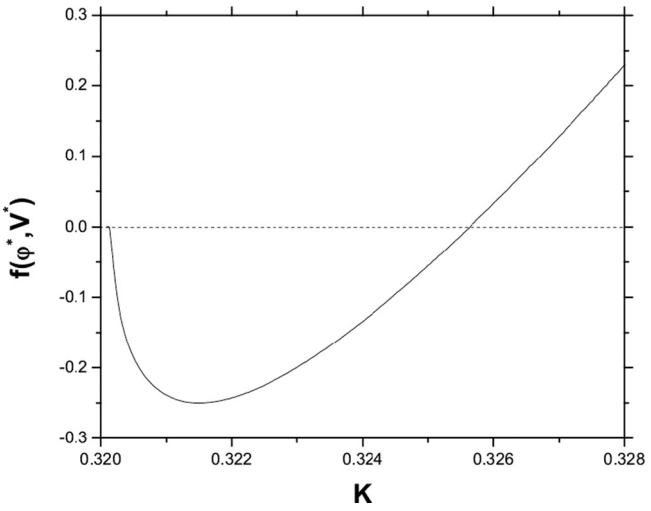

FIG. 6. Plot of Eq. (22). The K interval where the function $f(\varphi^*,V^*)$ is negative corresponds to the stable regime of the period-2 AM.

There is a crucial difference between the AM present in the complete and in the simplified model. Due to the symplectic feature of the simplified model, the corresponding AM constitute periodic islands when we plot the coordinate V modulated between [0,1]. So, the AM of the simplified model just affect the dynamics of initial conditions taken inside these special kinds of islands. On the other hand, the complete model is not area preserving and due to this reason the AM affect globally the dynamics of the system. However, the bifurcations and resonances suffered by the islands of acceleration in the simplified model correspond to changes on the global influence of the accelerating structure on the whole phase space of the complete model. Although the global status of the AM is always observed in complete bouncer model, for some K parameters, the initial conditions that are affected by this behavior may be different.

To demonstrate this we show in Fig. 7 a sequence of bifurcations and shape changes suffered by the island of acceleration of period-1, obtained by the simplified model. As this structure is located at $V = 1$ on the border of mod[1] phase space, Fig. 7 is shown as mod[2] phase space for a better visualization.

As one can see by comparing Fig. 4(a) with Figs. 7(b) and 7(c), the first decrease of the quantity $\langle V\rangle_{10^4}$ corresponds to a reduction of the island area due the ejection of the period-4 secondary chain of islands at the parameter $K \approx 0.5285$. After this ejection, the center of the accelerating island recovers its stability, as can be observed in Fig. 7(d) for the parameter $K \approx 0.54$. At this parameter value it is possible to see an increase of the quantity $\langle V\rangle_{10^4}$ observed in Fig. 4(a). A very strong resonance of the main island with a period-3 chain of islands can be observed in Fig. 7(e), where most of the stable area lies on the secondary chain rather then in the main island. The ejection of the period-3 secondary islands can be observed in Fig. 7(f), almost vanishing the area of acceleration. This phenomenon was also observed in standard map and called

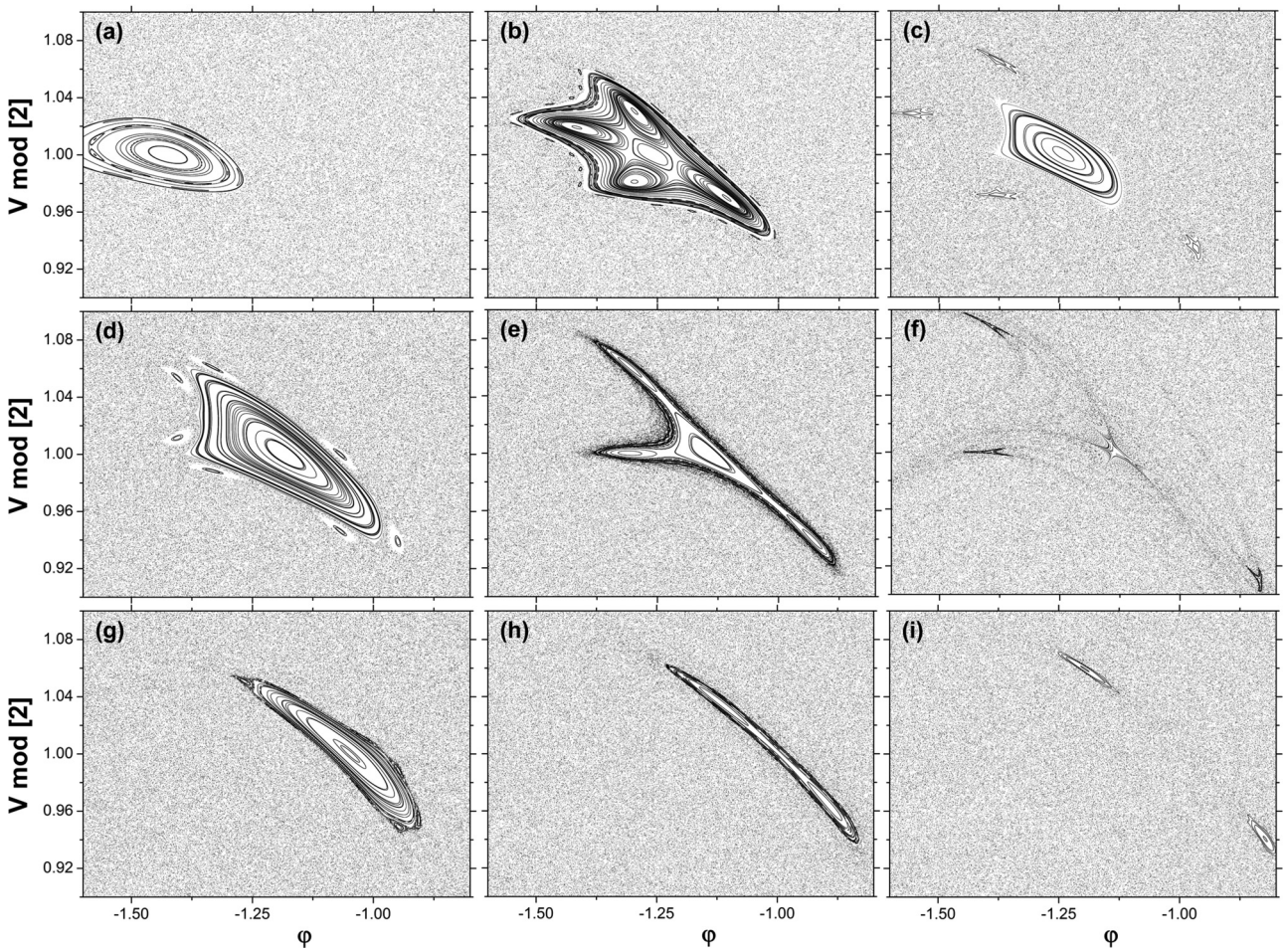

FIG. 7. Impact maps of simplified model in phase space V mod[2] versus ϕ around the period-1 acceleration island and control parameter (a) $K = 0.5055$, (b) $K = 0.5252$, (c) $K = 0.5285$, (d) $K = 0.54$, (e) $K = 0.5491$, (f) $K = 0.5530$, (g) $K = 0.5773$, (h) $K = 0.5958$, and (i) $K = 0.6012$.

"period-3 catastrophe" [40,43]. For the complete bouncer model we can associate this phenomenon to the drastic decrease in global acceleration of initial conditions, as can be observed at $K \approx 0.555$ in Fig. 4(a). Again, the increase of K parameter value restores the central island stability, which suffers a period-doubling bifurcation of its central fixed point at the parameter $K \approx 0.6$ given by Eq. (15).

As we can observe in Fig. 4(a), the K parameter associated with high values of the quantity $\langle V \rangle_{10^4}$ stands further than predicted by Eq. (15). Therefore, although the center of the accelerating island has undergone a bifurcation at K parameter value predicted by Eq. (15), the remaining islands from the bifurcation continue to affect the acceleration of some initial conditions near that region. When we continue to increase the value of K parameter, these trajectories are destroyed due to the natural period-doubling sequence. The same scenario of resonances and bifurcations is observed for the period-2 AM in the range of parameters $0.3205 \leqslant K \leqslant 0.326$, associated to the fluctuations observed in Fig. 4(b).

The period-4 AM in the parameter range $0.234 \leqslant K \leqslant 0.25$ shown in Fig. 4(c) experiences a different sequence of resonances and bifurcations. To exemplify this scenario, we show in Fig. 8 a sequence of phase space zoomed in one of the four islands of the period-4 AM.

One can observe in Figs. 8(a) and 8(b) that the first slight decrease of the quantity $\langle V \rangle_{10^4}$ observed in Fig. 4(c) is associated with a resonance between the central island and a period-3 secondary chain of islands. The ejection of the secondary islands does not represent an extinction of the stable island as occurred in Fig. 7(f). Instead, the first extinction of stable island occurs at $K \approx 0.2380$ as shown in Fig. 8(c) by a period-doubling bifurcation suffered by the central fixed point. This fixed point becomes hyperbolic and then, by the increase of K, becomes elliptical again at $K \approx 0.2389$ as can be seen at Fig. 8(d). After that, a new resonance with a period-3 secondary chain of islands causes a period-3 catastrophe at $K \approx 0.242$ as can be seen at the sequence of Figs. 8(e)–8(g). The period-3 catastrophe almost vanishes the stable island area and causes a dip of $\langle V \rangle_{10^4}$ on the curve of Fig. 4(c). At the sequence, the central fixed point recovers its stability and its the lost area as shown in Fig. 8(h). The final extinction of the AM is caused by another period-doubling bifurcation at $K \approx 0.2480$ as can be seen in Fig. 8(i).

IV. STRUCTURE OF ACCELERATION

We analyze how the velocities increase in the phase space with repetition of islands and structures by plotting the V

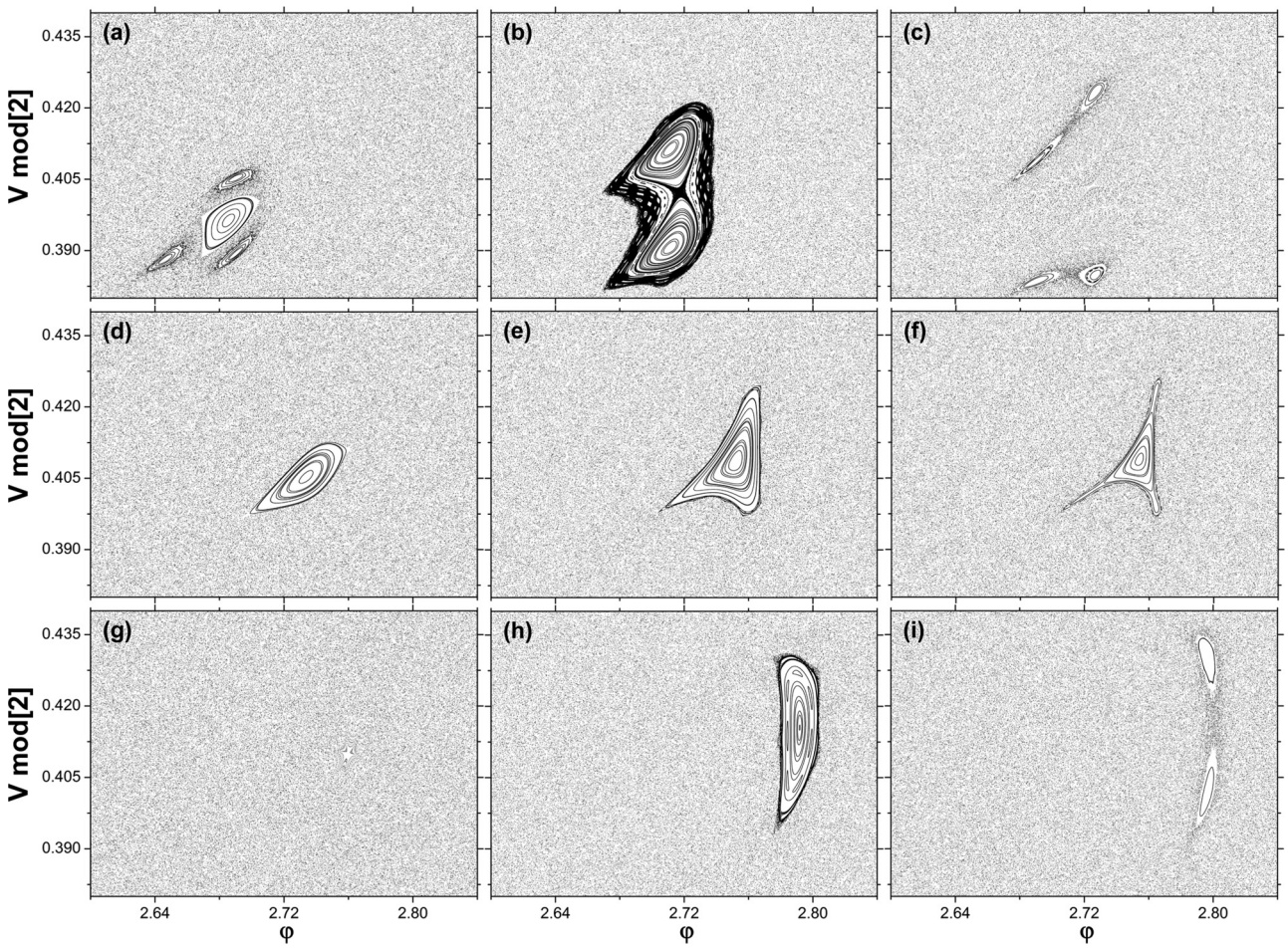

FIG. 8. Impact maps of simplified model in phase space V mod[1] vs ϕ around the period-3 acceleration island and control parameter (a) $K = 0.2354$, (b) $K = 0.2374$, (c) $K = 0.2380$, (d) $K = 0.2389$, (e) $K = 0.2409$, (f) $K = 0.2411$, (g) $K = 0.2418$, (h) $K = 0.2465$, and (i) $K = 0.2480$.

variable modulated between 0 and 1. Initially, for K parameters chosen from the intervals of Figs. 4(a)–4(c), in Figs. 9(a)–9(c) we represent points with the color blue (dark gray) or red (light gray) in phase space, for trajectories with Jacobian values smaller or larger than the unity, respectively.

A. Phase space

As can be seen in Fig. 9, there are regions in phase space with high and low concentration of points, indicated by circles and squares as the structures of acceleration and deacceleration, respectively. The regions of high concentration of points mean that the impacts for many different initial conditions happen at a same value of φ and the velocity V jumps regularly at each impact.

As the phase space is modulated in the V direction, the accelerating structure appears like an attractive fixed point. The deaccelerating structures have the same interpretation, but considering the backwards way map. When we consider the forward map, the deaccelerating structures in the modulated phase space can be seen as unstable regions acting to reduce the energy of the particle at each impact. The color division in the phase space reveals that the accelerating structures are located at shrinkage regions, while the deacceleration structures are located at expanding region of phase space. The regular islands are located partially at each region. As a consequence, the accelerating structures attract most of the initial conditions in the chaotic sea while the deaccelerating structures only influence the initial conditions very close to the periodic point at their centroid during a limited number of impacts.

As shown in Fig. 10, the DM and AM have different natures, as the first one takes the velocity down in a linear way, working as a repulsive point, the second one, accelerates the particle also in a linear way, acting as an attracting point or sink. Although we are dealing with a nondissipative system, we observe an asymptotic convergence. Such peculiar behavior is only observed considering modulated values of velocity. By considering the complete values of velocity, we have a linear growth or linear decay of this variable, depending on the AM or DM influences.

The curve shown in Fig. 10(a) shows a very special initial condition chosen exactly inside the DM, located near the $V \approx 180$. Once this DM has a repelling nature, we may see a decrease in the velocity until the orbit leaves the influence zone of the DM and reaches the chaotic sea, where its velocity grows, in average, with a power law exponent $\beta \approx \frac{1}{2}$. Also, we notice that the linear decay has a coefficient near $\frac{1}{3}$,

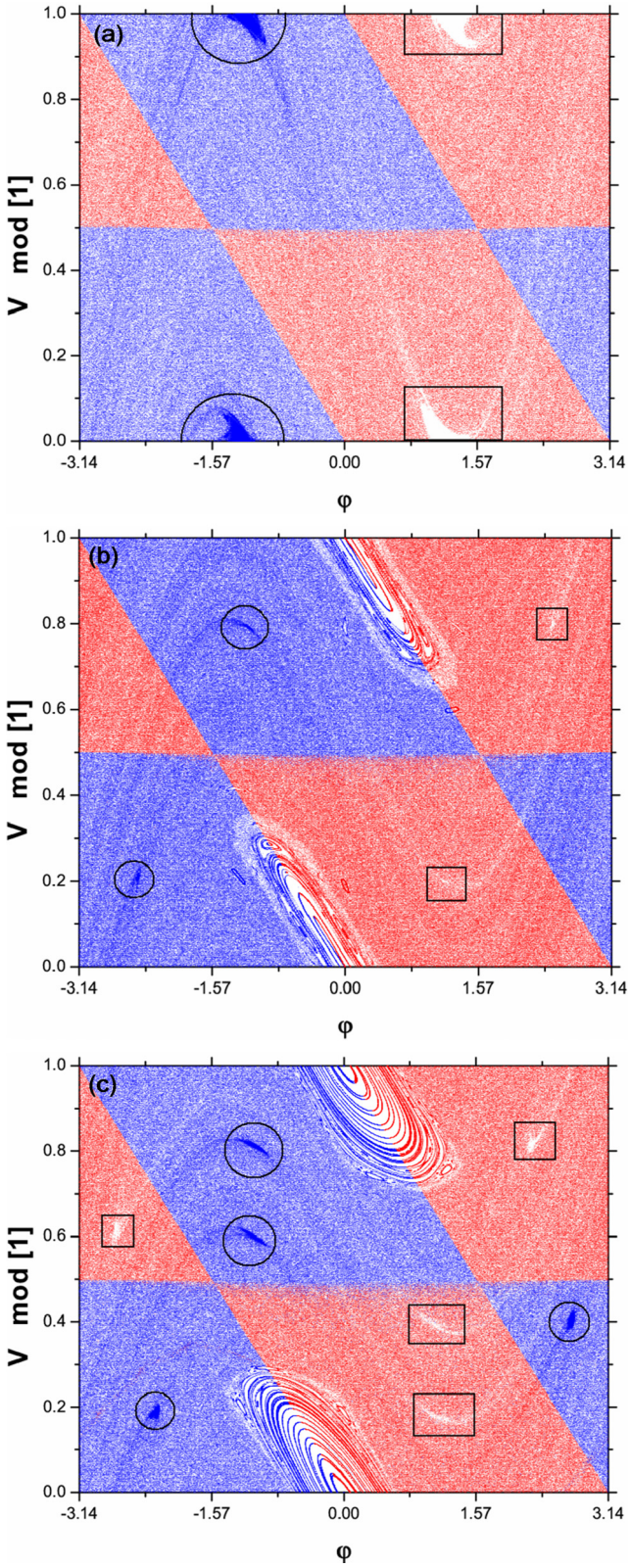

FIG. 9. (Color online) Impact map during 200 iterations of 80 initial conditions in phase space V mod[1] vs φ for control parameter (a) $K = 0.54$, (b) $K = 0.322$, and (c) $K = 0.237$. The blue (dark gray) region of phase space corresponds to Jacobian values smaller than the unity, while the red (light gray) regions correspond to values larger than the unity. The structures of accelerating are indicated by circles, while the deaccelerating structures are indicated by squares.

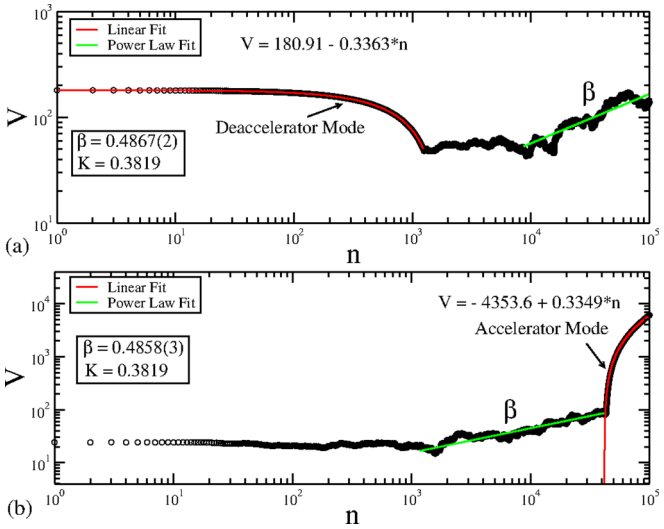

FIG. 10. (Color online) Evolution of a single initial condition as function of n. In (a), the initial condition was given right inside the DM, which explains the linear decay in the beginning of the dynamics. In (b), the initial condition was chosen in the chaotic sea. After some collisions, it finally enters in the domain region of the AM, which is represented by the linear growth in the end of the curve.

indicating that the parameter $K = 0.3819$ is associated with a period-3 DM. In Fig. 3, this structure can be identified as a less pronounced AM between the period-1 and period-2 indicated.

On the other hand, in Fig. 10(b), the initial condition was chosen in the chaotic sea, and after a few collisions, the orbit starts to grow with a power law exponent $\beta \approx \frac{1}{2}$, and suddenly it bends towards a linear growth regime. This linear growth is due to the presence of the AM in the system. Also, the linear growth has a coefficient $\approx \frac{1}{3}$, indicating that the AM has also the same period-3 of the DM. It is important to clarify that an orbit will only reach a DM if we give the initial condition inside its influence zone. After the orbit leaves this zone, it could converge to an influence zone of an AM.

To identify the DM and AM influence zones, we introduce Fig. 11. We said already that an orbit can reach a DM only if the initial condition was chosen right inside of it. In Fig. 11(a), it is shown a grid of 1000×1000 initial conditions, in a particular region of the phase space where DM is located for $K = 0.3819$, so a period-3. We establish a criteria to verify if an initial condition was under the influence of the DM: a decreasing velocity reached the condition $V \leqslant 64$ at the collision (n). This condition defines a hole, i.e., a region defined in phase space [25,49,50]. Once an orbit reaches it, we marked its iteration of escape, and start to iterate a new initial condition [25,49,50]. This characteristic escape collision is represented by a color gradient in the logarithmic scale of Fig. 11(a), where the red (gray) represents fast escape through the limit decreasing velocity and the DM itself, yellow and green (light gray) represent orbit under the the influence zone of the DM, and finally blue and black (dark gray) mean that the orbits never reached the hole, or took a long time to reach it.

Now, looking at Fig. 11(b), one can see the attracting nature of the AM, where a single initial condition was evaluated for $K = 1.001$, which means a period-1 AM. We can see the orbit

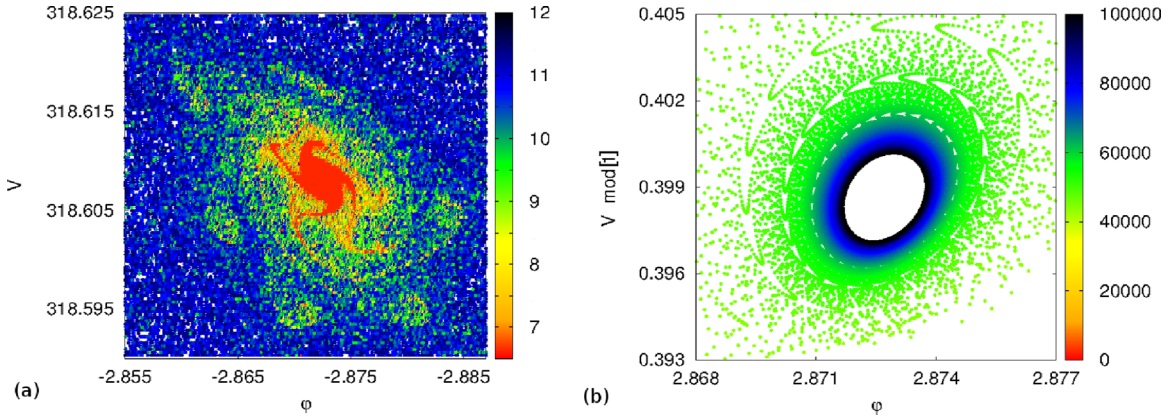

FIG. 11. (Color online) (a) Grid of initial conditions with and escape velocity $V = 64$. The logarithmic color scale shows the iteration of each initial condition had escaped through the hole, where red (gray) indicates fast escape or the DM itself; yellow and green (light gray) indicate the influence zone of the DM and blue and black (dark gray) orbits that never reached the escape velocity, or took a long time to do it. In (b), we show a zoom-in of the converging nature of the AM, where a single initial condition was iterated until 10^6 collisions, and converged to an asymptotic behavior. Here, the color scale represents the number of collisions. Also, in (b) the figure was made concerning the velocity axis taken mod[1].

converging to the point located in $V = 0.400$ and $\varphi = 2.725$. The color scale represents the number of collisions, where from green (light gray) to blue and black (dark gray) the collisions are increasing. It is good to emphasize that the plot of Fig. 11(b) was made concerning the velocity axis taken mod[1], and a zoom-in window was established in the region of the AM, that is the reason we may see a convergence instead of a growing behavior, as shown in Fig. 10(b).

B. Escape basin

The global feature of the AM in the complete bouncer model allows initial conditions far from the center of the accelerating structure to increase their velocities in a ballistic way. In other words, there exists a set of initial conditions that collapses into the accelerating structure, and this set varies its domain with the change of K. We call this set of initial conditions as the "escape basin" of the AM.

In this section, we investigate the relation between the escape basin of the period-1 AM with the stable and unstable manifolds in the phase space. First, to determine which initial condition collapses into the accelerating structure, we set a grid of $(10^4 \times 10^4)$ initial conditions in phase space and obtain the average acceleration associated with of each one by means of Eq. (10) after 10^3 iterations. We define the escape basin of the AM as the set of initial conditions whose final average velocity after 10^3 iterations ($\langle V \rangle_{10^3}$) is, at least, 93% of $\langle V \rangle_{10^3}$ at the center of the accelerating structure. After testing, we conclude that the difference of 7% between the center and the less accelerated initial condition is due to the maximum transient experienced by initial conditions that belong to the escape basins before their collapse into the center. In Fig. 12, we plot in black the escape basin of the period-1 AM at $K = 0.54$. We repeat the same procedure, considering the backward version of the map. The set of initial conditions accelerated in backwards maps represents the basin of the DM and is shown in red (gray) in Fig. 12.

The escape basin structure of both AM and DM can be explained by the stable and unstable invariant manifolds of hyperbolic points in the phase space. The invariant manifolds are sets of points whose forward and backward iterations belong to the same set. For stable manifold, forward iterations converge to a hyperbolic saddle point, while for unstable manifold, backward iterations converge to the hyperbolic saddle point, as the number of iterations goes to infinity. The nonuniformity in the invariant manifolds concentration is usually related with pronounced filaments of manifold branches that form a kind of escape channel, which drive particles to the high energy region of the phase space [51,52].

To explain the escape basin structure, we obtain the stable and unstable manifolds of the complete version of the bouncer model. A method to obtain a numerical approximation to these invariant manifolds is to consider the first n_0 (say, 10) forward and backward images of a set of a large number of initial

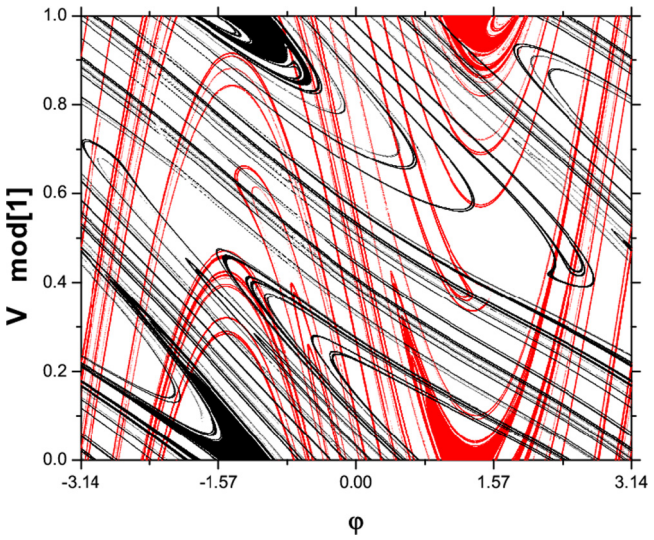

FIG. 12. (Color online) Escape basins of period-1 AM ($K = 0.54$) represented in black by initial conditions with $\langle V \rangle_{10}^3$ larger than 93% of $\langle V \rangle_{10}^3$ evaluated at the center of the accelerating structure. The same considering the backward map represented in red (gray) indicates the basin of the DM.

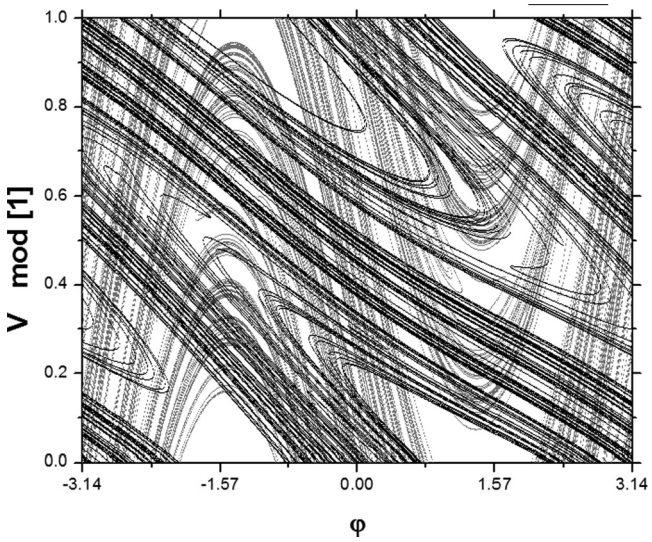

FIG. 13. Stable and unstable manifolds, represented respectively in black and gray, emanating from the saddle point at $(V^*;\varphi^*) = (0.549;\pi)$.

conditions (say, 10^7) over the eigendirections of the linearized system near a saddle point embedded in the chaotic sea. When the phase space is filled by chaotic orbits (global chaos), the invariant manifolds are indifferent to the specific saddle point chosen. For the case of parameter $K = 0.54$, we observe a global chaos in phase space as shown in Fig. 9(a), which allows us to choose arbitrarily the saddle point located at $(V^*;\varphi^*) = (0.549;\pi)$ to apply the procedure described. The resulting invariant stable and unstable manifolds are shown in Fig. 13 in black and gray, respectively. We can observe in this figure a good correspondence between Figs. 12 and 13. Actually, the accelerating structure fills the empty spaces left between the branches of the stable manifold while the deaccelerating structure fills the empty spaces left between the branches of the unstable manifold. These branches of manifolds act like a labyrinth path in the phase space, guiding the initial conditions until they reach the center of the accelerating structure, or the center of the deaccelerating structure, if the mapping were iterated backwards.

V. CONCLUSIONS

The dynamics of a bouncing-ball model was investigated under the influence of accelerating structures known as accelerator modes (AM). These modes appear in the dynamics only for a restricted range of the control parameter, which was analytically obtained in order to explain the accelerating scenario range. It was done for AM of different periods and their respective bifurcations.

When the dynamics is evaluated under the presence of these modes, the velocity of the particle increases in a regular and monotonic way, which gives us a linear growth of the mean velocity of an ensemble of particles. On the other hand, the velocity has a normal diffusive growth, according to a power law $\beta \approx \frac{1}{2}$. In some cases, we may have these two distinct regimes coexisting in the dynamics. This indicates that some initial conditions initiate their dynamics exhibiting FA and then collapse in an AM and begin to increase its velocity in a linear way. This feature was explained by the fact that the complete bouncer model is not symplectic. For this reason, the accelerating structure represents an attractive region on modulated phase space affecting globally the system dynamics. Complementary with the AM, we find in the antisymmetric position of them the so called deaccelerated modes, which have unstable nature. If an initial condition is given in the DM zone of influence, we observe a decay on the velocity. Also, we observed the existence of basins of acceleration and deacceleration, where their boundaries are drawn by the stable and unstable manifolds, respectively.

It would be interesting, in a close future, to investigate if these phenomena could be extended to other nondissipative vibrating and impact systems, as billiards. In time, we could try to extend the bouncing-ball model to a quantum version and verify if we would have the same effects observed in other quantum systems [53–55]. Also, due the global characteristics of the AM in this system, it could be used to investigate the distribution of the AM of different periods in the K parameter range. Until now, it was a challenging task using symplectic maps since the initial conditions tested are rarely located inside the islands of acceleration (which location is unpredictable in most of the cases). With a model that exhibits a global behavior for the AM, any sufficiently great ensemble of initial conditions could be used to identify the AM existence and its period.

ACKNOWLEDGMENTS

A.L.P.L. acknowledges FAPESP (Grant No. 2014/25316-3) and CNPq for financial support. I.L.C. thanks FAPESP (Grant No. 2011/19296-1) and E.D.L. thanks FAPESP (Grant No. 2012/23688-5), CNPq, and CAPES, Brazilian agencies.

[1] R. C. Hilborn, *Chaos and Nonlinear Dynamics: An Introduction for Scientists and Engineers* (Oxford University Press, New York, 1994).
[2] A. J. Lichtenberg and M. A. Lieberman, *Regular and Chaotic Dynamics*, Applied Mathematical Sciences, Vol. 38 (Springer, New York, 1992).
[3] G. M. Zaslasvsky, *Physics of Chaos in Hamiltonian Systens* (Imperial College Press, New York, 2007).
[4] G. M. Zaslasvsky, *Hamiltonian Chaos and Fractional Dynamics* (Oxford University Press, New York, 2008).
[5] K. T. Alligood, T. D. Sauer, and J. A. Yorke, *Chaos: An Introduction to Dynamical Systems* (Springer, New York, 1996).
[6] E. Fermi, Phys. Rev. **75**, 1169 (1949).
[7] M. A. Lieberman and V. A. Godyak, IEEE Trans. Plasma Sci. **26**, 955 (1998).
[8] A. V. Milovanov and L. M. Zelenyi, Phys. Rev. E **64**, 052101 (2001).
[9] A. Veltri and V. Carbone, Phys. Rev. Lett. **92**, 143901 (2004).
[10] K. Kobayakawa, Y. S. Honda, and T. Samura, Phys. Rev. D **66**, 083004 (2002).

[11] F. M. Rieger, V. Bosch-Ramon, and P. Duffy, Astrophys. Space Sci. **309**, 119 (2007).
[12] G. Lanzano *et al.*, Phys. Rev. Lett. **83**, 4518 (1999).
[13] F. Saif, I. Bialynicki-Birula, M. Fortunato, and W. P. Schleich, Phys. Rev. A **58**, 4779 (1998).
[14] A. Steane, P. Szriftgiser, P. Desbiolles, and J. Dalibard, Phys. Rev. Lett. **74**, 4972 (1995).
[15] A. Loskutov, A. B. Ryabov, and L. G. Akinshin, J. Exp. Theor. Phys. **89**, 966 (1999).
[16] A. Loskutov, A. B. Ryabov, and L. G. Akinshin, J. Phys. A: Math. Gen. **33**, 7973 (2000).
[17] R. E. de Carvalho, F. C. Souza, and E. D. Leonel, Phys. Rev. E **73**, 066229 (2006).
[18] F. Lenz, F. K. Diakonos, and P. Schmelcher, Phys. Rev. Lett. **100**, 014103 (2008)
[19] E. D. Leonel, D. F. M. de Oliveira, and A. Loskutov, Chaos **19**, 033142 (2009).
[20] A. L. P. Livorati, A. Loskutov, and E. D. Leonel, Physica A (Amsterdam) **391**, 4756 (2012).
[21] V. Gelfreich, V. Rom-Kedar, K. Shah, and D. Turaev, Phys. Rev. Lett. **106**, 074101 (2011).
[22] V. Gelfreich, V. Rom-Kedar, and D. Turaev, Chaos **22**, 033116 (2012).
[23] K. Shah, D. Turaev, and V. Rom-Kedar, Phys. Rev. E **81**, 056205 (2010).
[24] B. Batistić, Phys. Rev. E **90**, 032909 (2014).
[25] A. L. P. Livorati, T. Kroetz, C. P. Dettmann, I. L. Caldas, and E. D. Leonel, Phys. Rev. E **86**, 036203 (2012).
[26] P. J. Holmes, J. Sound Vibration **84**, 173 (1982).
[27] L. D. Pustilnikov, Theor. Math. Phys. **57**, 1035 (1983).
[28] R. M. Everson, Physica D (Amsterdam) **19**, 355 (1986).
[29] D. Sternad, M. Duarte, H. Katsumata, and S. Schaal, Phys. Rev. E **63**, 011902 (2000).
[30] N. A. Burnham, A. J. Kulik, G. Gremaud, and G. A. D. Briggs, Phys. Rev. Lett. **74**, 5092 (1995).
[31] F. Spahn, U. Schwarz, and J. Kurths, Phys. Rev. Lett. **78**, 1596 (1997).
[32] P. Muller, M. Heckel, A. Sack, and T. Poschel, Phys. Rev. Lett. **110**, 254301 (2013).
[33] F. Pacheco-Vazquez, F. Ludewig, and S. Dorbolo, Phys. Rev. Lett. **113**, 118001 (2014).
[34] A. C. J. Luo and R. P. S. Han, Nonl. Dyn. **10**, 1 (1996).
[35] J. J. Barroso, M. V. Carneiro, and E. E. N. Macau, Phys. Rev. E **79**, 026206 (2009).
[36] L. Mátyás and R. Klanges, Physica D (Amsterdam) **187**, 165 (2004).
[37] E. D. Leonel and A. L. P. Livorati, Commun. Nonl. Sci. Num. Simul. **20**, 159 (2015).
[38] T. L. Vincent and A. I. Mees, Int. J. Bifurcation Chaos Appl. Sci. Eng. **10**, 579 (2000).
[39] S. K. Joseph, I. P. Mario, and M. A. F. Sanjuán, Commun. Nonl. Sci. Num. Simul. **17**, 3279 (2012).
[40] A. J. Lichtenberg, M. A. Liberman, and N. W. Murray, Physica D (Amsterdam) **28**, 371 (1987).
[41] A. J. Lichtenberg and M. A. Liberman, Physica D (Amsterdam) **33**, 211 (1988).
[42] Y. H. Ichikawa, Y. Nomura, and T. Kamimura, Prog. Theor. Phys. Suppl. **99**, 220 (1989).
[43] Y. H. Ichikawa, T. Kamimura, T. Hatori, and S. Y. Kim, Prog. Theor. Phys. Suppl. **98**, 1 (1989).
[44] G. M. Zaslavsky and B. A. Niyazov, Phys. Rep. **283**, 73 (1997)
[45] V. Rom-Kedar and G. M. Zaslavsky, Chaos **9**, 697 (1999).
[46] S. T. Dembinski and P. Peplowski, Phys. Rev. E **55**, 212 (1997).
[47] T. Manos and M. Robnik, Phys. Rev. E **87**, 062905 (2013).
[48] T. Manos and M. Robnik, Phys. Rev. E **89**, 022905 (2014).
[49] E. G. Altmann, J. S. E. Portela, and T. Tél, Rev. Mod. Phys. **85**, 869 (2013).
[50] A. L. P. Livorati, O. Georgiou, C. P. Dettmann, and E. D. Leonel, Phys. Rev. E **89**, 052913 (2014).
[51] T. Kroetz, M. Roberto, E. C. Silva, I. L. Caldas, and R. L. Viana, Phys. Plasmas **15**, 092310 (2008).
[52] J. D. Szezech Jr., I. L. Caldas, S. R. Lopes, R. L. Viana, and P. J. Morrison, Chaos **19**, 043108 (2009).
[53] M. K. Oberthaler, R. M. Godun, M. B. d'Arcy, G. S. Summy, and K. Burnett, Phys. Rev. Lett. **83**, 4447 (1999).
[54] S. Schlunk, M. B. d'Arcy, S. A. Gardiner, and G. S. Summy, Phys. Rev. Lett. **90**, 124102 (2003).
[55] S. Fishman, I. Guarneri, and L. Rebuzzini, J. Stat. Phys. **110**, 911 (2003).